



3-D numerical analysis of natural convective liquid cooling of a 3×3 heater array in rectangular enclosures

S.K.W. Tou*, C.P. Tso, X. Zhang

School of Mechanical and Production Engineering, Nanyang Technological University, Nanyang Avenue, North Spine (N3), Level 2, Singapore 639798

Received 18 August 1998; received in revised form 30 November 1999

Abstract

The paper presents a three-dimensional (3-D) computational study of natural convection cooling on a 3-by-3 array of discrete heat sources flush-mounted on one vertical wall of a rectangular enclosure filled with various liquids ($Pr = 5, 9, 25$ and 130) and cooled by the opposite wall. The non-dimensional governing equations with appropriate boundary conditions are solved in the primitive variable form employing a semi-implicit finite volume formulation. The procedures are validated experimentally and numerically with published results. Computations are performed for a range of modified Rayleigh numbers from 10^4 to 10^8 while the enclosure aspect ratio varies from 1 to 20. The effects of modified Rayleigh number, enclosure aspect ratio and Prandtl number on heat transfer characteristics are investigated. The results reveal that the flow field is complex and the heat transfer from the discrete heaters is not uniform. The row-averaged Nusselt number increases with Rayleigh number in the power of 0.27. It also increases with enclosure aspect ratio in the range of 1–3 and attains the maximum when aspect ratio is greater than ~ 3 . The heater surface temperature is the highest at the top-row heaters regardless of the modified Rayleigh number and enclosure aspect ratio. The effects of Prandtl number are negligible in the range from 5 to 130. © 1999 Elsevier Science Ltd. All rights reserved.

1. Introduction

The conventional method of cooling by either free or forced convection of ambient air is no longer adequate to cope with the high heat flux generated by IC chips [1,2]. In the past decades, a significant amount of research has been devoted to the development of electronic cooling technology employing dielectric coolants. The research shows that the indirect liquid cooling has failed to meet the harsh thermal require-

ments due to poor thermal conductance at the solid–solid interface. Following the successful introduction of direct liquid immersion cooled supercomputers in the late 80's, the Cray-2 and the ETA-10, it has led some observers to suggest that direct cooling with inert, dielectric liquids may become the solution for computers in the late 90's. However, direct liquid cooling technology has not gained widespread popularity due to the lack of understanding of the transport phenomena using dielectric coolants and numerous parameters are involved. It is noticed that 3-D numerical studies on natural convection liquid cooling are rare as compared to its counterpart on forced convec-

* Corresponding author.

Nomenclature

A	enclosure aspect ratio (height-to-width ratio)
A_h	heat source area
E, I, b	heat source location
C	depth of enclosure along y -axis
D	width of enclosure along x -axis
g	gravitational acceleration
h	heat transfer coefficient
H	height of enclosure along z -axis
k	thermal conductivity
L_z, L_x	square heat source length
Nu_1	Nusselt number based on length of heat source
p	dynamic pressure
P	dimensionless dynamic pressure
Pr	Prandtl number
q''	heat flux [W m^{-2}]
Ra	modified Rayleigh number
S_x	heater pitch in the span-wise (x)-direction
S_z	heater pitch in the stream-wise (z)-direction
T	fluid temperature
T_c	cold wall temperature
u	velocity in x -direction
U	dimensionless velocity in x -direction
v	velocity in y -direction
V	dimensionless velocity in y -direction
w	velocity in x -direction
W	dimensionless velocity in z -direction
x	x coordinate
X	dimensionless coordinate in x -direction
y	y coordinate
Y	dimensionless coordinate in y -direction
z	z coordinate
Z	dimensionless coordinate in z -direction.

Greek symbols

α	thermal diffusivity
β	thermal expansion coefficient
θ	dimensionless temperature
μ	dynamic viscosity
ν	fluid kinematic viscosity
ρ	fluid density
ρ_0	fluid density at cold wall temperature
ϕ	general variable.

tion liquid cooling. Several numerical analyses have been carried out to investigate some of the parameters that affect the natural convective heat transfer from arrays of heaters in an enclosure [3–11].

A natural convective mode of heat transfer is favored wherever possible and there is a need for a better understanding on the transport processes in order to take advantage of the scheme. With this mo-

tion, the present work is initiated to investigate the single-phase natural convective transport phenomena in a liquid filled enclosure with arrays of discrete heat sources using a 3-D numerical model. The objective is to extend the study to cover a wider range of Rayleigh number ($Ra=10^4$ – 10^8) and Prandtl number ($Pr=5$ – 130) and to examine the effects of the enclosure aspect ratio ($A=1$ – 20) that have not been reported.

2. Model formulation

2.1. Governing equations and assumptions

The non-dimensional governing equations in Cartesian form for the present study are the continuity, momentum and energy equations:

$$\frac{\partial U}{\partial X} + \frac{\partial V}{\partial Y} + \frac{\partial W}{\partial Z} = 0 \tag{1}$$

$$U \frac{\partial U}{\partial X} + V \frac{\partial U}{\partial Y} + W \frac{\partial U}{\partial Z} = -\frac{\partial P}{\partial X} + Pr \left[\frac{\partial^2 U}{\partial^2 X} + \frac{\partial^2 U}{\partial^2 Y} + \frac{\partial^2 U}{\partial^2 Z} \right] \tag{2}$$

$$U \frac{\partial V}{\partial X} + V \frac{\partial V}{\partial Y} + W \frac{\partial V}{\partial Z} = -\frac{\partial P}{\partial Y} + Pr \left[\frac{\partial^2 V}{\partial^2 X} + \frac{\partial^2 V}{\partial^2 Y} + \frac{\partial^2 V}{\partial^2 Z} \right] \tag{3}$$

$$U \frac{\partial W}{\partial X} + V \frac{\partial W}{\partial Y} + W \frac{\partial W}{\partial Z} = -\frac{\partial P}{\partial Z} + Pr \left[\frac{\partial^2 W}{\partial^2 X} + \frac{\partial^2 W}{\partial^2 Y} + \frac{\partial^2 W}{\partial^2 Z} \right] + Ra Pr \theta \tag{4}$$

$$U \frac{\partial \theta}{\partial X} + V \frac{\partial \theta}{\partial Y} + W \frac{\partial \theta}{\partial Z} = \frac{\partial^2 \theta}{\partial^2 X} + \frac{\partial^2 \theta}{\partial^2 Y} + \frac{\partial^2 \theta}{\partial^2 Z} \tag{5}$$

where the non-dimensional parameters are defined as follows:

$$Ra = gq''L_z^4\beta/(k\nu\alpha), \quad Pr = \nu/\alpha, \quad U = uL_z/\alpha,$$

$$V = vL_z/\alpha, \quad W = wL_z/\alpha$$

$$X = x/L_z, \quad Y = y/L_z, \quad Z = z/L_z, \quad P = p/(\rho_0(\alpha/L_z)^2),$$

$$\theta = (T - T_c)/(q''L_z/k).$$

It can be seen, from the above governing equations, that the modified Rayleigh number and Prandtl number are two of the important model parameters for a given flow geometry. In the model development, fluid is assumed to be isotropic and the Boussinesq approximation applies. It is also assumed that there is no source/sink in the system at steady-state condition and that fluid properties remain unchanged. The heat transfer characteristics are described by the Nusselt number with is defined as follows:

- The local Nusselt number:

$$Nu_{L_z}(x,z) = \frac{q''L_z}{(T(x,z)|_{y=0} - T_c)k} = \frac{1}{\theta|_{y=0}}. \tag{6}$$

- The average Nusselt number:

$$\begin{aligned} \overline{Nu}_{L_z(i,j)} &= \frac{q''L_z}{k} \frac{1}{\frac{1}{A_h} \int_{A_h} (T(x,z)|_{y=0} - T_c) dA_h} \\ &= \frac{1}{\frac{1}{A_h} \int_{A_h} \theta|_{y=0} dA_h}. \end{aligned} \tag{7}$$

2.2. Model geometry and parameters

Figs. 1 and 2 illustrate a schematic sketch and the physical dimensions of the simulated rectangular enclosure which is similar to the experimental arrangements of [12] and [10,11]. The enclosure is defined with respect to a Cartesian coordinate *X–Y–Z* with the *Z*-axis pointing upwards. A 3 × 3 array (12.7 × 12.7 × 9.5 mm) composed of discrete, flush-mounted, iso-flux heat sources is installed on one of the vertical walls while the opposite wall is treated as an isothermal surface maintained at a lower temperature. The discrete heat sources are identical and are of square shape (12.7 mm). Each heat source consumes an equal amount of heat energy and generates a uniform heat flux *q''* which can be varied as desired. The remaining walls are assumed adiabatic. The middle *Y–Z* plane located at center-line (*x* = *D*/2, *y* = *C*/2) is taken as the *X–Z* plane of symmetry because symmetry has been observed in previous numerical work [5,9,13] and is also experimentally confirmed by others [10,14,15]. The flow geometry is characterized by the enclosure aspect ratio which is the only geometric parameter that is varied in the study. Table 1(a) summarizes the fixed and variable geometric parameters.

Simulations are performed with water, FC-72, FC-77 and ethylene glycol corresponding to *Pr* = 5, 9, 23 and 130, respectively. The modified Rayleigh number is varied from 10⁴ to 10⁸ by changing the heat supply to the heaters. Table 1(b) gives the ranges of these two model parameters used in the study.

2.3. Boundary conditions

The boundary conditions are as follows:

$$\text{At } X = 0: \quad P = 0, \quad \frac{\partial \theta}{\partial X} = 0, \quad U = V = W = 0. \tag{8}$$

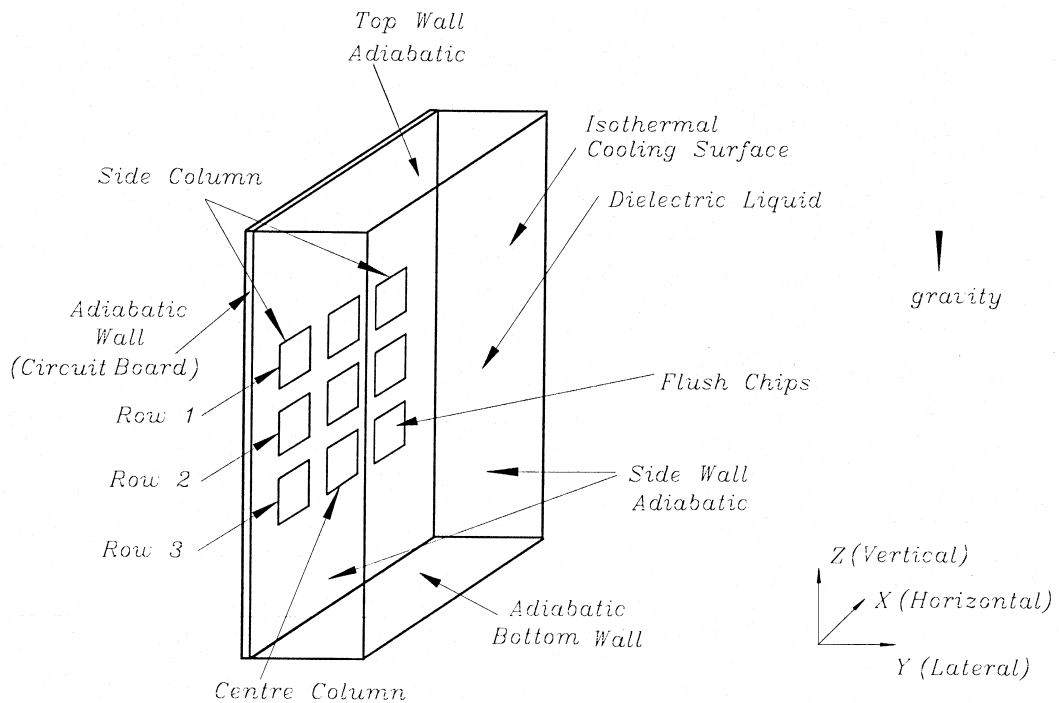


Fig. 1. Enclosure geometry.

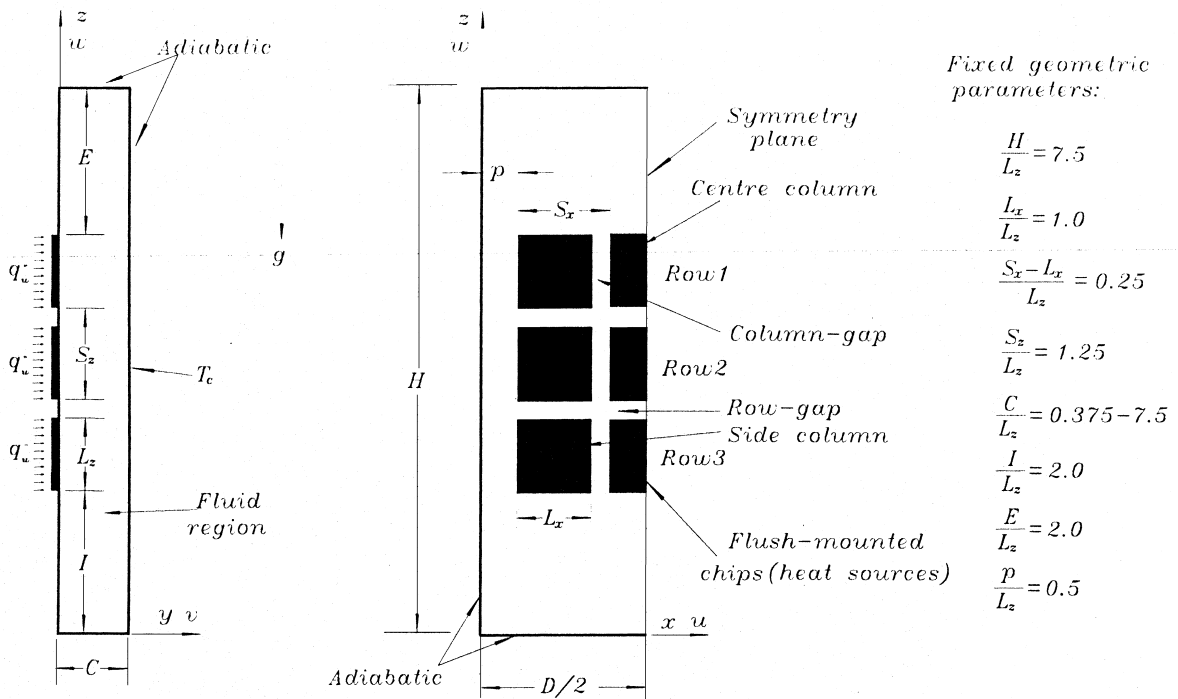


Fig. 2. Sectional-view of enclosure with discrete heat sources.

Table 1
Summary on geometric parameters (a) and model parameters (b)

(a) Fixed geometric parameters $H=95.3$ mm, $D=57.2$ mm; $L_z=L_x=12.7$ mm							Variable geometric parameter
H/L_z	L_x/L_z	$(S_x - L_x)/L_z$	S_x/L_z	I/L_z	E/L_z	b/L_z	Enclosure aspect ratio $A = H/C$
7.5	1.0	0.25	1.25	2.0	2.0	0.5	1.0–20.0
(b) Prandtl number Pr							Modified Rayleigh number Ra
5, 9, 25 and 130							10^4 – 10^8

$$\text{At } X = \frac{D}{2L_z} = 2.25: \quad \frac{\partial P}{\partial X} = 0, \quad \frac{\partial \theta}{\partial X} = 0, \tag{9}$$

$$U = \frac{\partial V}{\partial X} = \frac{\partial W}{\partial X} = 0.$$

$$\text{At } Y = 0: \quad \frac{\partial \theta}{\partial Y} = -1, \tag{10}$$

for the iso-flux region (heater)

$$\frac{\partial \theta}{\partial Y} = 0, \quad \text{for the adiabatic region (the rest)} \tag{11}$$

$$P = 0, \quad U = V = W = 0. \tag{12}$$

$$\text{At } Y = \frac{C}{L_z} = 0.375 \rightarrow 7.5: \quad P = 0, \quad \theta = 0, \tag{13}$$

$$U = V = W = 0.$$

$$\text{At } Z = 0 \quad \text{and} \quad Z = \frac{H}{L_z} = 7.5: \quad P = 0, \tag{14}$$

$$\frac{\partial \theta}{\partial Z} = 0, \quad U = V = W = 0.$$

3. Numerical method and model validation

A 3-D, non-uniform and staggered grid is used with a control volume formulation in accordance with the SIMPLE algorithm. The power law scheme is employed for the convective-diffusive transport variables. Pressure-correction and velocity-correction schemes are implemented in the model algorithm to arrive at a converged solution when both the pressure and velocity satisfy the momentum and continuity equations. For non-linear problems, under-relaxation is employed to avoid divergence in the iterative solutions by first selecting an under-relaxation factor to calculate a weighted average of the newly calculated

value and the previous value at each point. The effect of under-relaxation factor on convergence rate is considerable. Unacceptably slow convergence or divergence of the solution is obtained if the factor is too low or too high. In the present study, strong under-relaxation is found to be required for the velocities, particularly on the W -component because of the strong source term resulted from the buoyancy source term. On the other hand, temperature requires only minor under-relaxation. It is recommended that a relaxation factor of about 0.3–0.5 is to be used for the velocity components while a factor of about 0.4–0.6 is adequate for the pressure and temperature solutions. The resulting set of discretized equations for each variable are solved by the line-by-line procedure which is the combination of the Tri-Diagonal Matrix Algorithm (TDMA) and the Gauss-Seidal iteration technique with additional block-corrected method for fast convergence. For each modified Rayleigh number, the converged solution obtained from a lower modified Rayleigh number is used as the initial guess for the next round of computation to reduce the computational times. At high modified Rayleigh numbers, it was found that severe under-relaxation was required to obtain convergence.

To determine whether the converged solutions correspond physically to the steady solutions, an unsteady version of the code has been used to check the results at high modified Rayleigh numbers, i.e., 10^7 and 10^8 . The unsteady code is fully implicit in time and uses the same iteration scheme as the steady version of the code to obtain convergence within a given time step. Convergence for a given time step is assumed when the changes in temperature and velocities between successive iterations, for all grid points, is less than $0.001 \times$ the maximum value of the dependent variables at that time step. The convergence criterion for the steady state is that the changes in all dependent variables between successive time steps, for all grid points, is less than $0.0001 \times$ the maximum value of the dependent variables.

A 3-D, non-uniform and staggered grid is used to discretize the physical domain. Grid independence is

established by examining the heat transfer from the surfaces of the heat sources. Test runs are performed on a series of non-uniform grids to determine the grid size effects. Since a wide range of modified Rayleigh number is considered, the tests are conducted for three modified Rayleigh numbers at 10^5 , 10^6 and 10^7 . The maximum difference in the row-averaged Nusselt number between grid $(37 \times 31 \times 61)$ and grid $(95 \times 31 \times 91)$ is 4.0% for Row 3 at $Ra=10^5$. The difference in the row-averaged Nusselt number between grid $(55 \times 31 \times 91)$ and grid $(95 \times 31 \times 91)$ is less than 0.35%. Thus, the former grid $(55 \times 31 \times 91)$ is used in subsequent computations.

The numerical procedures are first validated using an experimental cubical enclosure with $\theta=0$ at $Y=1$, and $\theta=1$ at $Y=0$. The modified Rayleigh number is assumed to be 10^6 and the Prandtl number is 0.7, corresponding to one of the cases investigated by Lankhorst and Hoogendoorn [16]. Numerical results are subsequently compared in Fig. 3 with the experimental data of [12] and [17] for different enclosure width and Prandtl number. Another comparison is also made with respect to the experimental work by Fusegi et al. [13]. The results are all in excellent agreement. The model is also validated numerically by comparing with those of Heindel et al. [10] and is shown in Fig. 3. Comparison of results shows the maximum deviation is within 4.5%. By extrapolating in Fig. 3, the Nusselt number is not approaching one but the same order of magnitude when the modified Rayleigh num-

ber decreases to zero as the limiting case for pure conduction.

4. Results and discussions

4.1. 3-D nature of flow field

The model results show that the flow field is complex and only discussed briefly. The 3-D nature of the flow field is presented in Fig. 4 for a test case with $Ra=10^7$, $Pr=9$ and $A=7.5$ which shows the variations of velocity profiles across the enclosure at various elevated sections. The W -component is much greater than the other two and represents the primary fluid motion in the enclosure. The strength of W -component is however very weak at the bottom region ($Z \sim 1.0$) indicating that fluid is practically stagnant. Adjacent to the heated wall, fluid driven by buoyancy force begins to accelerate from the bottom and set up the primary flow in the vertical upward direction. Maximum velocities across the heater array are attained in all three columns at about the mid-section ($Z \sim 3.0$). The W -component bifurcates towards the ceiling and bottom noticeably in the enclosure central region (between $Y=0.2$ and $Y=0.8$) and a flat-profile takes shape whereby forming a pair of weak, rotating cells. On approaching the ceiling ($Z \sim 6.5$), the rising plume begins to decelerate and flow across the enclosure towards the cold wall. Some of the fluids also bifurcate upon impingement with the ceiling, but they eventually

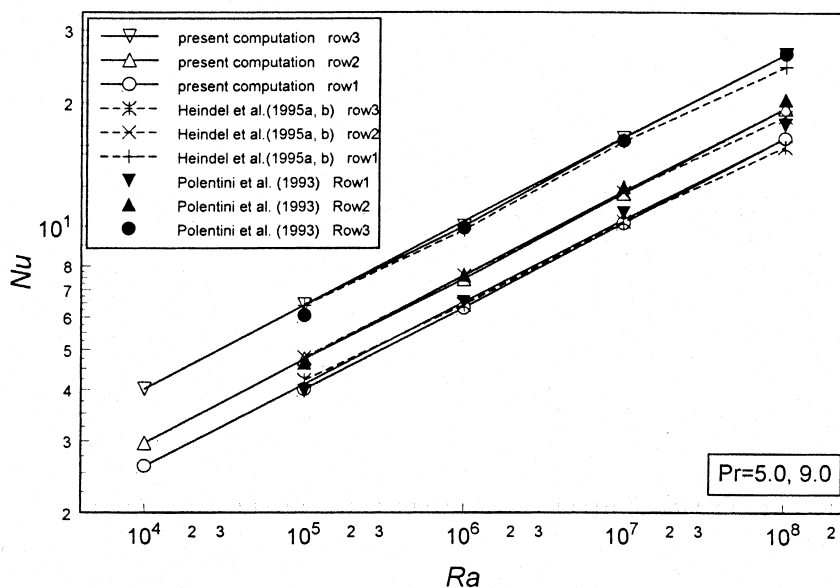


Fig. 3. Comparison of row-averaged Nusselt number.

sweep towards the cold wall by the bulk fluid motion. Adjacent to the cold wall, the primary flow is downward. As a result, two main opposite streams are formed in the enclosure being separated roughly by the mid-plane at centerline ($Y=0.5$).

The velocity profiles for the U -component and V -component are also shown in Fig. 4 which reveals

complex flow patterns are inevitable as the profiles change shapes drastically from one elevated section to another. In addition, flow reverses its direction rapidly as the sign alternates between positive and negative. Although the U -component and V -component are small in magnitude, they combine with the primary flow (W -component) and the resulting flow is a pair of

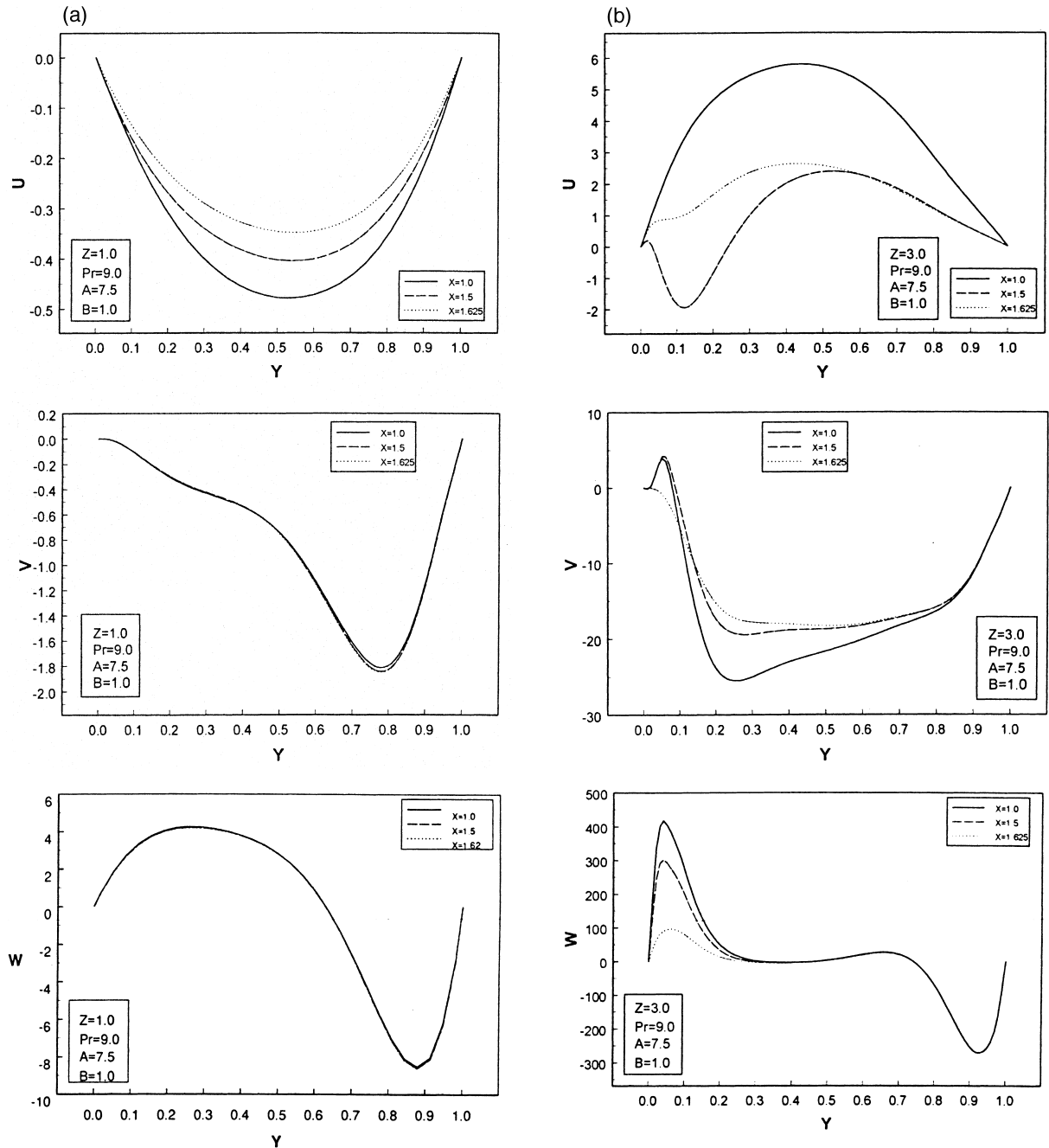


Fig. 4. (a) U , V , W velocity profiles at $Z=1.0$. (b) U , V , W velocity profiles at $Z=3.0$. (c) U , V , W velocity profiles at $Z=6.5$.

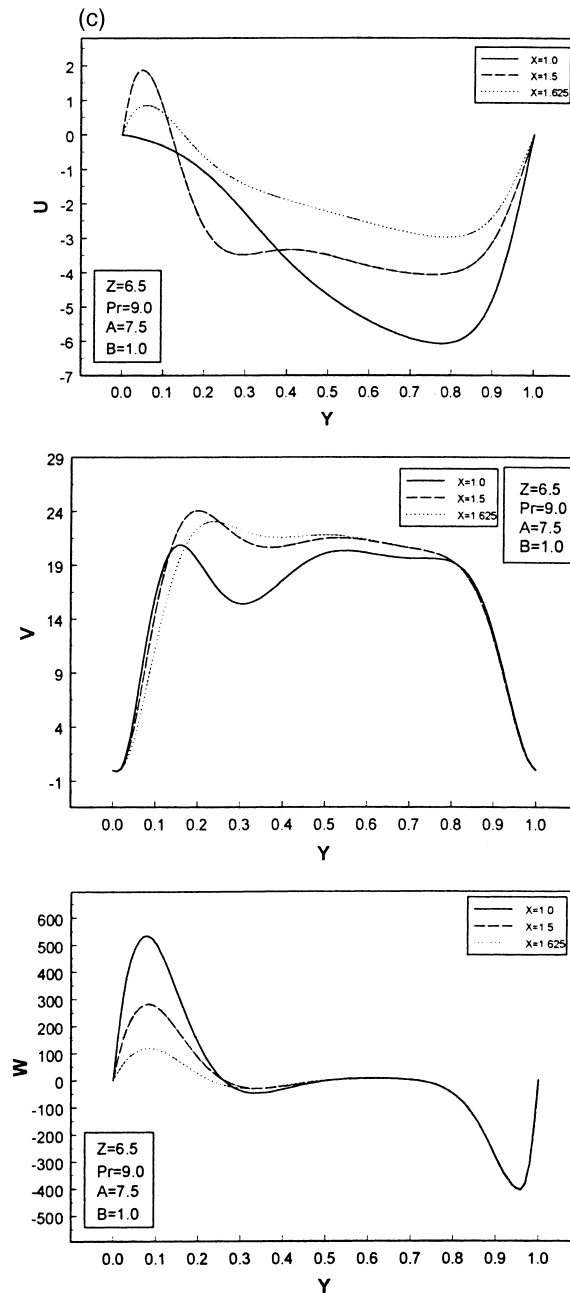


Fig. 4 (continued)

counter-rotating helical cells separated by the mid-plane.

4.2. Temperature field and heat transfer

The nature of the temperature fields is illustrated in Fig. 5 for the case with $Ra=10^7$, $Pr=9.0$ and $A=7.5$. The important parameter of practical interest in elec-

tronics cooling application is the maximum surface temperature (hot spot) on the discrete heater, which in the present simulations is seen to occur at the top row because fluid motion is weak and the local bulk fluid temperature is high in the ceiling. On the other hand, the heater surface temperature is the lowest at the bottom row where the local bulk fluid temperature is the lowest.

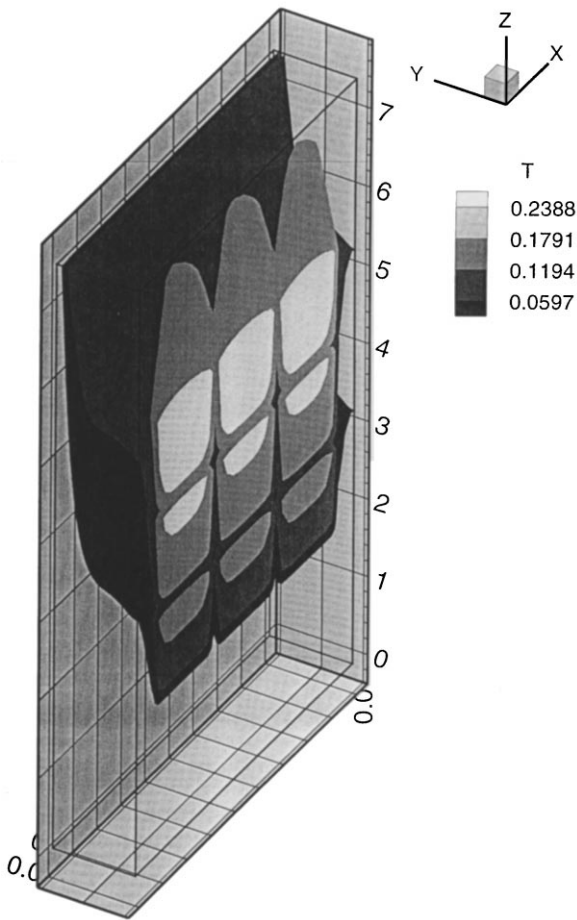


Fig. 5. Temperature field at $Ra = 10^7$, $Pr = 9$ and $A = 7.5$.

The spatial variation of local Nusselt number predicted by the present model at selected X locations are presented in Fig. 6. It can be seen that the local Nusselt number decreases monotonously from the maximum at the leading edge towards the trailing edge in all heaters. The local Nusselt number is also non-uniform across the heater span and attains the maximum at the heater edges ($X = 0.5$ and $X = 1.5$).

4.3. The effects of modified Rayleigh number

For simplicity only the W -velocity component, representing the primary flow, is used in Fig. 7 to illustrate the effects of modified Rayleigh number on the flow field for a fixed Prandtl number ($Pr = 9$) and geometry ($A = 7.5$). The W -velocity component is very weak everywhere in the enclosure when $Ra < 10^5$. Under this condition, natural convective heat transfer is not effective and conduction mode prevails. The W -velocity component increases in strength with Rayleigh number as the buoyancy force begins to dominate the fluid motion and thus convective heat transfer becomes effective. When $Ra > 10^7$, the W -velocity component begins to bifurcate in the enclosure central region (between $Y = 0.2$ and $Y = 0.8$) and a flat-velocity profile takes shape whereby forming a pair of rotating cells. The strength of this pair of cells is much less than the main helical cells whose sizes have nevertheless been reduced and are now confined to the hot wall ($Y = 0 - 0.2$) and the cold wall ($Y = 0.8 - 1.0$), respectively.

Temperature isotherms on the $X-Z$ planes at selected Y locations are shown in Fig. 8 for a range of modified Rayleigh numbers. The hot spots are sup-

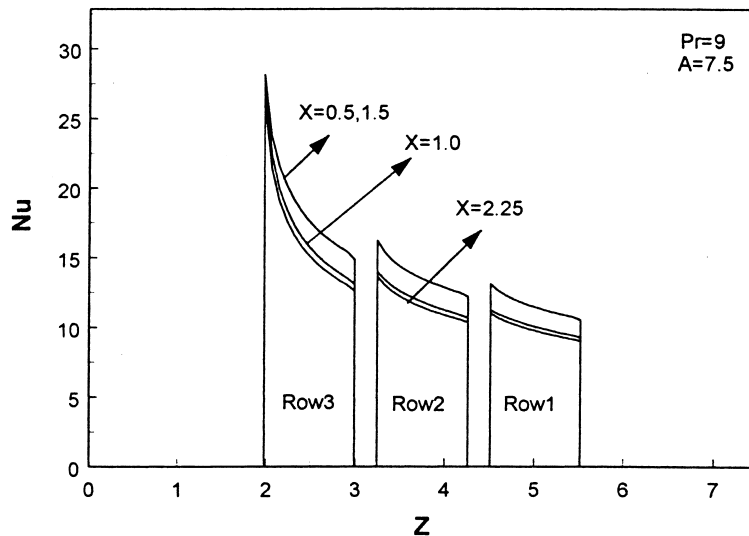


Fig. 6. Spatial variation of local Nusselt number at selected X locations with $Ra = 10^7$.

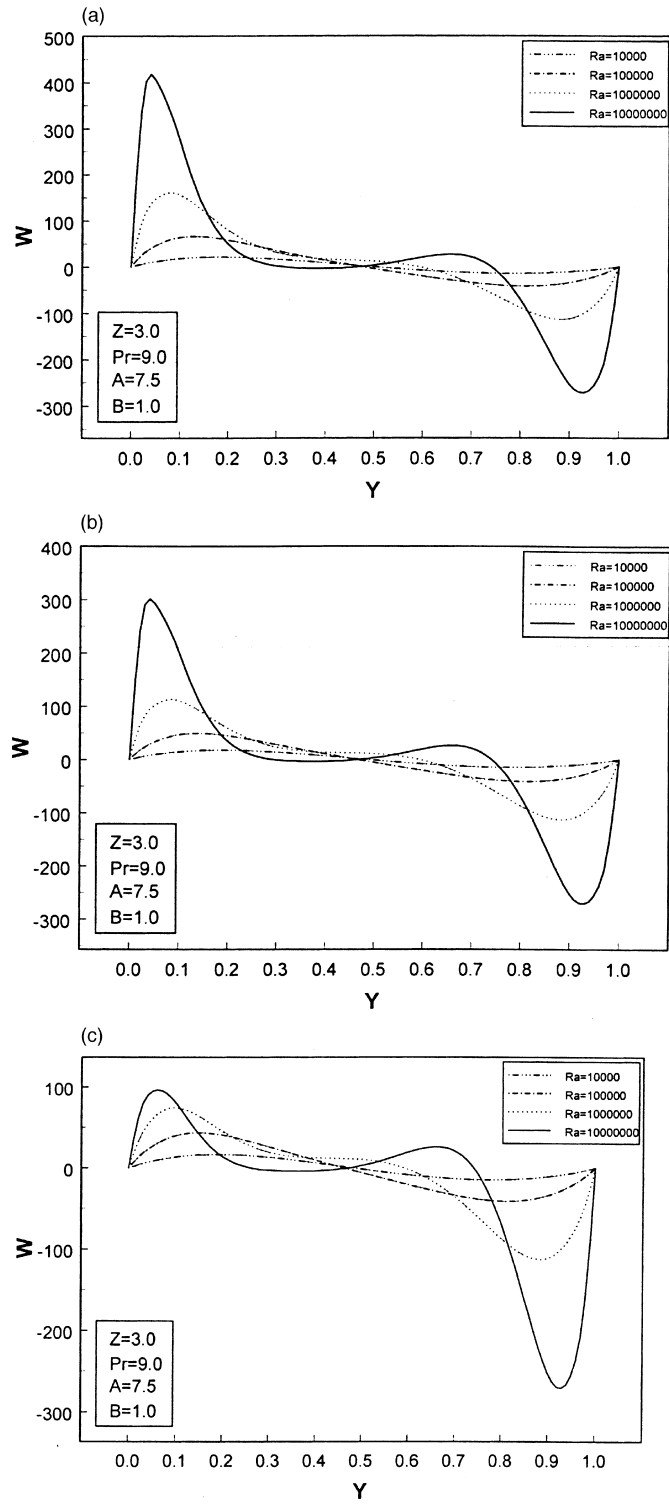


Fig. 7. W -velocity profiles at $Z=3.0$ and selected X locations for different Rayleigh number. (a) $X=1.0, Z=3.0$. (b) $X=1.5, Z=3.0$. (c) $X=1.625, Z=3.0$.

pressed and shift towards the ceiling as the modified Rayleigh number increases. Furthermore, thermal stratification expands from the enclosure bottom into the mid-section.

The important effects of modified Rayleigh number on heat transfer are reflected on the row-averaged Nusselt number which are illustrated in Fig. 3. This figure reveals that the row-averaged Nusselt number increases with modified Rayleigh number in the power of 0.27. The modified Rayleigh number has been extended to a wider range of 10^4 – 10^8 as compared to others [10–12]. For comparison, the experimental data of Polentini et al. [12] and Heindel et al. [11] are also shown in the same figure. The maximum deviation between the computational and experimental results is 8.06% and occurs at $Ra = 10^8$ at the top-row heaters.

4.4. The effects of enclosure aspect ratio

To examine the effects of enclosure aspect ratio, computations are carried out for a dielectric fluid FC-72 ($Pr=9.0$) with enclosure aspect ratio, $A=1.0, 1.5, 2.0, 5.0, 7.5$ and 20.0 while other geometry remain unchanged. Numerical results are obtained for range

of modified Rayleigh numbers from 10^5 – 10^7 . Again, only the W -component is used in Fig. 9 to illustrate the effects of enclosure aspect ratio on fluid flow inside the enclosure. As the enclosure aspect ratio reduces, the hot wall and cold wall are farther apart and become less dependent on each other. Flow tends to be confined to the opposite walls leaving the central region practically stagnant.

Fig. 10 illustrates the effects of aspect ratio on the row-averaged Nusselt number. The row-averaged Nusselt number attains the maximum value in the range of enclosure aspect ratios from 3 to 20. It begins to decrease as the enclosure aspect ratio varies from 3 to unity. This suggests that $A \approx 3$ is the optimal enclosure aspect ratio to get maximum heat transfer from the discrete heaters. It is also noted from the same figure that, for a given modified Rayleigh number, the lowest row-averaged Nusselt number is at the top-row heaters and the highest row-averaged Nusselt number is at the bottom-row heaters, respectively. This means the highest heater surface temperature occurs at the top-row heaters regardless of the enclosure aspect ratio. This figure also shows that the effects of enclosure aspect ratio on the row-averaged Nusselt number

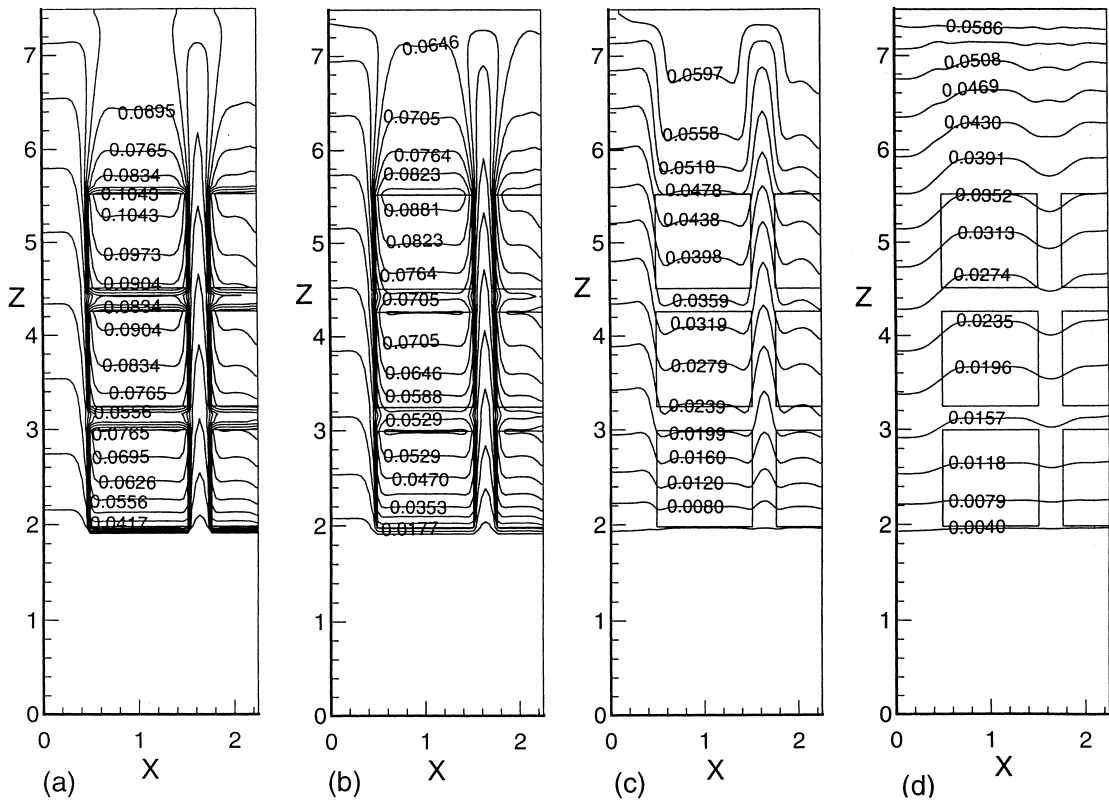


Fig. 8. Isotherms on the X - Z planes at selected Y locations for $Ra=10^7$, $Pr=9$ and $A=7.5$: (a) $Y=0$; (b) $Y=0.035$, (c) $Y=0.1$; (d) $Y=0.2$.

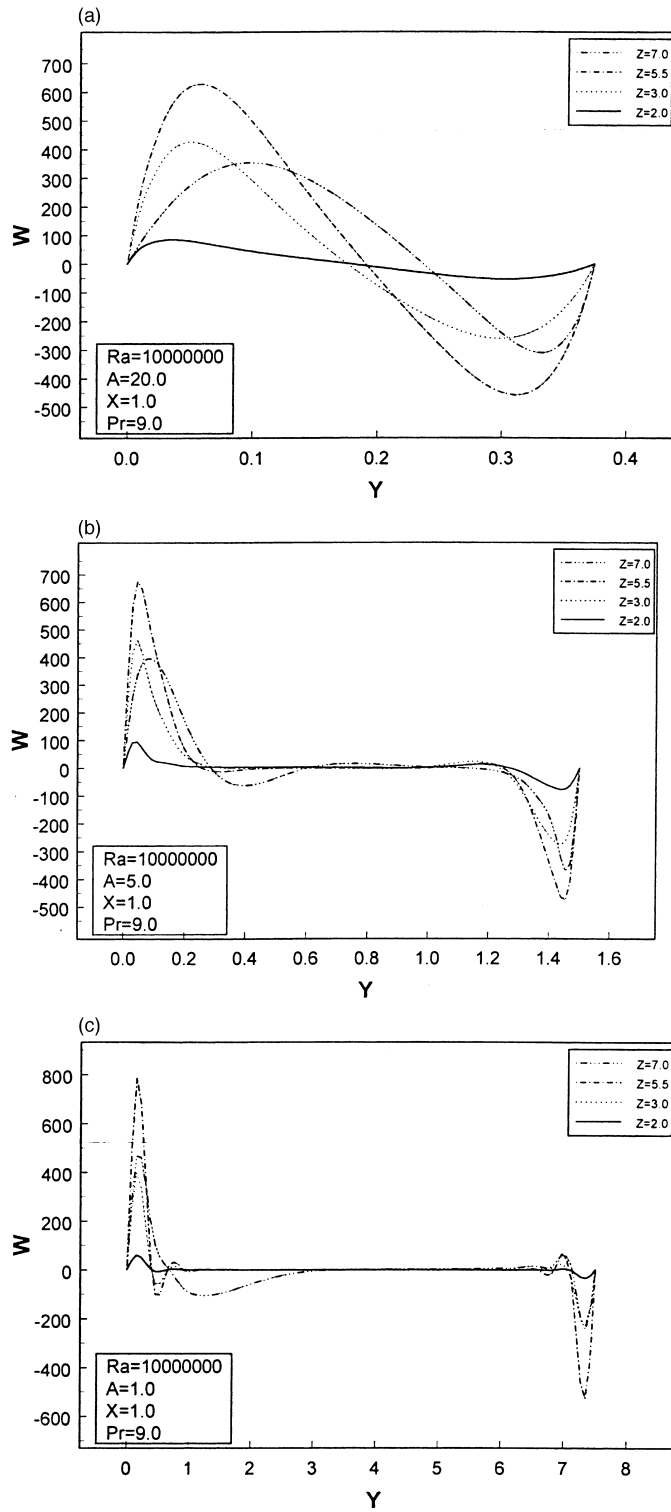


Fig. 9. Effects of enclosure aspect ratio on W -velocity profiles at different Z elevations for $X=1.0$, $Ra=10^7$ and $Pr=9.0$: (a) $A=20.0$; (b) $A=5.0$; (c) $A=1.0$.

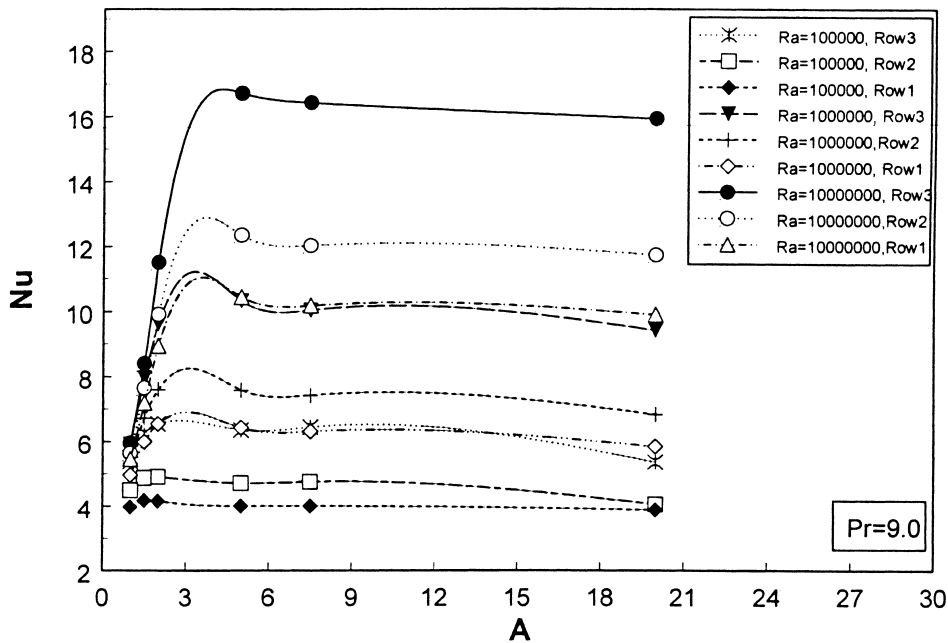


Fig. 10. Effects of enclosure aspect ratio on the row-averaged Nusselt number.

tend to degrade with decreasing modified Rayleigh number.

4.5. The effects of Prandtl number

Computations are carried out for various fluids (water, dielectric fluorinerts and ethylene glycol) corresponding to $Pr=5, 9, 25$ and 130 , respectively. It is found that, with other parameters unaltered, Prandtl number has a negligible effect on heat transfer and fluid flow. This indicates that the results obtained from water would be applicable to the dielectric liquids as well. This allows the use of water to study dielectric liquids provided the flow geometry and other non-dimensional parameters are similar.

5. Conclusions

- The flow field, driven by buoyancy force, is complex since it is affected by the temperature field inside the enclosure. The modified Rayleigh number and 3-D enclosure geometry also play a key role in setting up pairs of counter-rotating helical cells.
- At low modified Rayleigh number ($< 10^5$), fluid is practically stagnant. As the modified Rayleigh number increases, the primary flow strengthens and is confined to the two opposite walls and a pair of weak rotating cells form in the central region. The

row-averaged Nusselt number increases with modified Rayleigh number in the power of 0.27 .

- Heat transfer from discrete heaters is non-uniform and should be accounted for by applying the averaging techniques. Maximum heat transfer occurs at the heater leading and side edges. The heater surface temperature is the highest at the top-row heaters and the lowest at the bottom regardless of the modified Rayleigh number and enclosure aspect ratio.
- The row-averaged Nusselt number attains the maximum value in the range of enclosure aspect ratio from 3 to 20. It begins to decrease as enclosure aspect ratio varies from 3 to unity. This optimal enclosure aspect ratio ($A \approx 3$) should be observed in packaging design. The effects of enclosure aspect ratio on the row-averaged Nusselt number tend to degrade with decreasing modified Rayleigh number.
- The effects of Prandtl number are negligible in the range from 5 to 130. This allows the use of liquids such as water for studying other dielectric liquids provided the flow geometry and other non-dimensional parameters are similar.

References

- [1] F.P. Incropera, Convection heat transfer in electronic equipment cooling, *J. Heat Transfer* 110 (1988) 1097–1111.

- [2] A. Bar-Cohen, Thermal management of electronic components with dielectric liquids, in: Proceedings of the ASME/JSME Thermal Engineering Joint Conference, 1991.
- [3] D. Kuhn, P.H. Oosthuizen, Three-dimensional transient natural convective flow in a rectangular enclosure with localized heating. *ASME*, 1986; *HTD-Vol. 63*, pp. 55–62 1986.
- [4] M. Afrid, A. Zebib, Three-dimensional laminar and turbulent natural convection cooling of heated blocks, *Numerical Heat Transfer Part A* 19 (1991) 405–424.
- [5] D. Wroblewski, Y. Joshi, Transient natural convection from a leadless chip carrier in a liquid filled enclosure: a numerical study. *Advances in Electronic Packaging; ASME, EEP-Vol. 1-1*, pp. 235–248 1992.
- [6] D. Mukutmoni, Y.K. Joshi, M.D. Kelleher, Computations for a three-by-three array of protrusions cooled by liquid immersion: effect of enclosure width. *Solutions to CFD Benchmark Problems in Electronic Packaging; ASME HTD-Vol. 255*, pp. 45–56 1993a.
- [7] D. Mukutmoni, Y.K. Joshi, M.D. Kelleher, Computations for a three-by-three array of protrusions cooled by liquid immersion: effect of substrate thermal conductivity. *Advances in Electronic Packaging; ASME EEP-Vol. 4-2*, pp. 745–753 1993b.
- [8] D. Wroblewski, Y.K. Joshi, Computations of liquid immersion cooling for a protruding heat source in a cubical enclosure, *Int. J. of Heat and Mass Transfer* 36 (5) (1993) 1201–1218.
- [9] D. Wroblewski, Y.K. Joshi, Liquid immersion cooling of a substrate-mounted protrusion in a three-dimensional enclosure: the effects of geometry and boundary conditions, *ASME, Journal of Heat Transfer* 116 (1994) 112–119.
- [10] T.J. Heindel, F.P. Incropera, Laminar natural convection in a discretely heated cavity: assessment of three-dimensional effects, *ASME, Journal of Heat Transfer* 117 (1995) 902–909.
- [11] T.J. Heindel, F.P. Incropera, Conjugate natural convection from an array of discrete heat sources: two- and three-dimensional model validation, *International Journal of Heat Transfer and Fluid Flow* 16 (1995) 501–510.
- [12] M.S. Polentini, S. Ramadhyani, F.P. Incropera, Single-phase thermosyphon cooling of an array of discrete heat sources in a rectangular cavity, *Int. J. of Heat and Mass Transfer* 36 (1993) 3983–3996.
- [13] T. Fuseqi, J.M. Hyun, K. Kuwahara, B. Farouk, A numerical study of three-dimensional natural convection in a differentially heated cubical enclosure, *Int. J. Heat and Mass Transfer* 34 (1991) 1543–1557.
- [14] H. Ozoe, N. Sato, S. Churchill, Experimental confirmation of the three-dimensional helical streaklines previously computed for natural convection in inclined rectangular enclosures, *International Chemical Engineering* 19 (1979) 454–462.
- [15] W.J. Hiller, S. Koch, T.A. Kowalewski, Three-dimensional structures in laminar natural convection in a cubic enclosure, *Experimental Thermal and Fluid Science* 2 (1989) 34–44.
- [16] A.M. Lankhorst, C.J. Hoogendoorn, Three-dimensional calculations of high Rayleigh number natural convection flows in enclosed cavities, in: Proceedings of National Heat Transfer Conference; Houston, Texas, 3, 1988, pp. 463–470.
- [17] V. Prasad, M. Keyhani, R. Shen, Free convection in a discretely heated vertical enclosure: effects of Prandtl number and cavity size, *ASME Journal of Electronic Packaging* 112 (1990) 63–74.